Journal of Structural Geology, Vol. 5, No. 2, pp. 181 to 195, 1983
Printed in Great Britain

0191-8141/83 $3.00+0.00

Strain analysis of deformed granitic rocks (Helikian), Muskoka District, Ontario

DONALD M. DAVIDSON, JR.*

Department of Geological Sciences, University of Texas, El Paso, TX 79968, U.S.A.

(*Received* 11 *November* 1981; *accepted in revised form* 19 *December* 1982)

Abstract—Three-dimensional analysis of irrotational, longitudinal, finite strain was carried out on samples from a crescentic sheet which intruded and was deformed with a host gneiss unit of probable Helikian age. Analytical methods were compared using deformed feldspar grains representing four ideal degrees of strain intensity observed in the porphyritic sheet. The polar plot and R_f/ϕ, R_s methods proved most reliable and sensitive.

Data derived from fabric and strain analysis at 38 sites in the units suggest a two-stage deformational sequence. The first stage produced recumbent, isoclinal, similar (class 2) folds with northwest-trending hinge surface traces. This fold form was modified during the second stage to produce an overall type 2 fold interference pattern. The second stage produced upright, open buckle folds as well as the resultant strain fabric currently observed. Strain analysis confirms the general fold geometries of the model, and also documents competency contrasts between the matrix and feldspar grains with increased strain intensity and magnitude. Deformation of feldspar grains in the sheet involved modification of a fabric of low strain magnitude ($\epsilon_s = 0.3$) and a k value near unity to magnitudes of $\epsilon_s = 2.6$ and $k = 0.6$. Matrix strain intensities and magnitudes are consistently higher than those of the feldspar markers in the sheet. This variation is related to competency differences between the matrix and the feldspar grains. Fabric anisotropy accounts for the strain gradient observed between the sheet and gneiss.

INTRODUCTION

ALTHOUGH the quantitative determination of strain in rocks has developed considerably during the past two decades (Tobisch *et al.* 1977, Ramsay & Wood 1973), applications of quantitative strain determinations in igneous rocks have generally been confined to volcanic rather than to intrusive bodies. Moreover, studies of intrusive bodies have often focused on mylonites or shear zones within such units (Ramsay & Graham 1970, Potter 1976, Themistocleous & Schwerdtner 1977, Nicolas *et al.* 1977, Burg & Laurent 1978, Ramsay & Allison 1979) or on regional fabric studies (Coward & James 1974).

Studies of overall strain distribution within deformed intrusives, particularly those that are porphyritic, are rare (Allison 1975, Schwerdtner *et al.* 1977, Schwerdtner *et al.* 1979, Davidson 1980). This is not surprising when one considers the general paucity of natural strain indicators, the absence of reference horizons such as bedding, and the possibility of significant contrast in behaviour between phenocrysts (strain markers) and matrix during deformation owing to ductility contrasts.

Despite such limitations, the present study was undertaken: (1) to determine whether a reasonably well-exposed (in two-dimensions) deformed intrusive could be quantitatively analysed for strain; (2) to detail the methods of study; (3) to compare the results for several analytical techniques on different strain markers within the body and (4) to resolve the strain history (kinematics) of the body if possible. This investigation was undertaken in the belief that studies of deformed intrusives may prove useful in unravelling the tectonic history of orogenic areas and those of Precambrian terrains, in particular.

Geologic setting

The study area is located in southeast Ontario (Fig. 1;

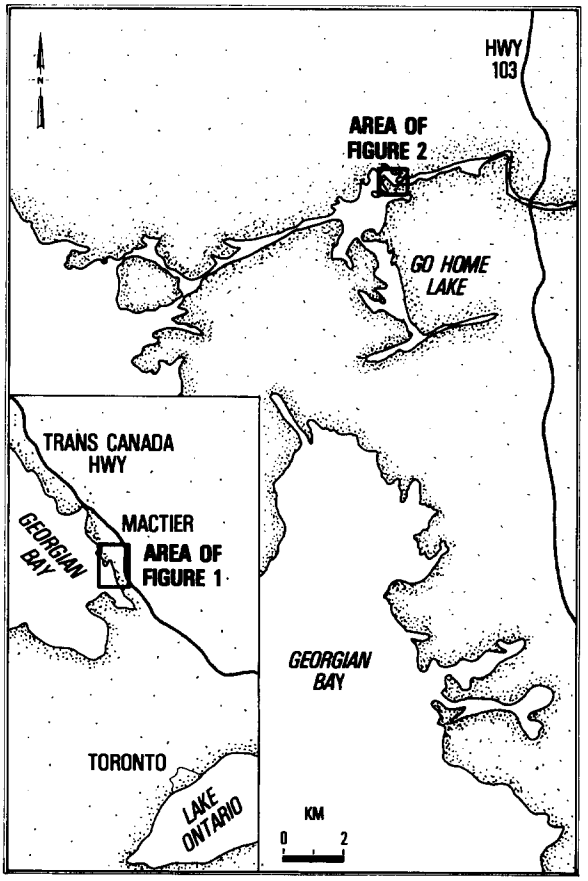

Fig. 1. Location map of the Flatrock Rapids area, Muskoka District, Ontario.

* Present address: Exxon Production Research, P.O. Box 2189, Houston, TX 77001, U.S.A.

also Muskoka Sheet, Ontario; 1:250,000). The region has been mapped at a scale of 1 inch equals 2 miles by Hewitt (1967) in a reconnaissance fashion while more detailed investigations within the Parry Sound–Huntsville area have been carried out by Bennett (1975) and Harrison (1976). The present study involved mapping approximately 2 km^2 in one month's field time by pace and compass method at a scale of 1:360 using an enlarged aerial photographic base.

The map area, as shown in Fig. 2, is part of a multiply deformed migmatitic gneiss terrain (Hewitt 1967). Schwerdtner & Waddington (1978) noted major northwest trending F_2 axial surface of type 2 and 3 fold interference patterns (Ramsay 1967) adjacent to the map area (near Bala); Lumbers (1974) mapped numerous type 2 interference fold patterns in the Burwash district, 50 km to the north with traces of F_2 fold surfaces trending N 30–50° W. The rocks in the study area are believed to be of Helikian age (1.6–0.9 Ga) and deformed during the Grenville (1.1–0.9 Ga) orogeny (Wynne-Edwards 1972), although Harrison (1976) identified an earlier, Elsonian (1.5–1.3 Ga) deformation in the region.

Table 1. Average modes (volume per cent) for gneiss and amphibolite units, Go Home Lake, Muskoka District, Ontario (based on 600 counts per thin section of amphibolite; and 1000 counts per thin section of gneiss)

	Gneiss (14 samples)		Amphibolite (7 samples)	
	Average	Range	Average	Range
Quartz	30.9	15–43		
K-Feldspar*	15.4	1–50	7.5	1–13
Microcline	21.9	2.55		
Plagioclase	9.9	1–50	18.2	10–35
Per cent An.	14	3–22	16	3–20
Antiperthite	0.48	tr-7	19.6	1–41
Biotite	13.6	5–30		
Hornblende	4.5	1–12	29.9	13–45
Diopside			4.7	1–13
Hypersthene			1.0	tr-7
Sphene	0.35		4.6	0.3–9
Apatite	0.4		0.2	
Zircon	0.2		0.3	
Epidote	1.3			
Opaque	0.36		6.2	
Other	0.71†		7.8‡	
	100		100	

* Most frequent value K-feldspar plus microcline = 37.3%.
† Chlorite, clinozoisite.
‡ Garnet, quartz, biotite.

PETROLOGY

Four major lithological units were mapped in the area: (1) a quartzo-feldspathic gneiss; (2) the Flatrock Rapids Sheet (FRS), a granite body, which is believed to have intruded the gneiss; (3) amphibolite which occurs as inclusions in both the gneiss unit and the FRS and (4) pegmatite dykes and sills which intruded all other units.

The host unit into which the FRS was intruded is a quartz–feldspar–biotite gneiss which is similar, although not identical, in composition to the intruding granite (see Tables 1 and 2). This medium- to coarse-grained rock contains K-feldspar porphyroblasts up to 3 cm long which vary in spatial distribution throughout the unit. The porphyroblasts are abundant (up to 35%) near the contact with the FRS and decreasing to 2–3% where observed up to 2 km away. The abundance of these grains also varies greatly (3–25%) over distances of the order of 10 cm across foliation in the gneiss unit. Although the presence of these feldspar porphyroblasts made local distinctions between the host rock and the granite difficult, the units were distinguishable by the presence of ubiquitous clear blue-grey quartz 'eyes' observed in the FRS only.

The FRS is a concordant body 750 m long and up to 150 m wide which is crescentic in shape and trends approximately N 20° W, parallel to the regional foliation (Fig. 2). Contact relationships between the sheet and the gneiss unit appear concordant owing to sub-parallel foliations in both rock types, and chilled contacts were not observed.

The sheet is composed of a coarse-grained, porphyritic alkali granite (Table 2) according to the classification of Streckeisen (1967). Microcline, orthoclase and quartz are found as phenocrysts which vary in size and form

Table 2. Average modes (volume per cent) of the Flatrock Rapids Sheet, Muskoka District, Ontario (based on 1000 counts per thin section)

	P_1 (1 sample)		P_2 (3 samples)		P_2–P_3 (4 samples)		P_3 (9 samples)		P_3–P_4 (5 samples)		P_4 (2 samples)		Total (24 samples)
	Av.	Range	Av.	Range	Av.	Range	Av.	Range	Av.	Range	Av.	Range	
Quartz	25.7		30.5	23–38	27.6	20–32	28.4	20–40	29.6	25–32	25.2	23–26	27.8
Plagioclase	2.6		4.5	4–5	4.7	4–5	7.6	1–17	11.0	8–15	5.3	4–6	6.0
Per cent An.	17		16		16		16		17		17		
Orthoclase*	51.0		22.9	8–32	13.5	10–16	18.8	5–48	16.0	10–20	12.7	9–12	22.5
Microcline	2.0		27.3	10–42	31.8	20–42	21.5	2–35	23.2	20–30	35.6	30–41	23.6
Biotite	12.5		7.6	6–12	10.6	8–12	13.1	5–20	10.8	8–13	13.0	13	11.3
Hornblende	4.3		4.7	3–7	8.1	1–14	6.5	2–15	6.5	2–12	4.2	1–8	5.7
Sphene	1.0		1.5		1.2		1.3		0.6		0.5		0.9
Zircon	0.1		0.3		0.8		0.4		0.2		tr		0.3
Apatite	0.3		tr		0.7		0.9		0.3		0.5		0.5
Opaque	0.2		0.3		0.5		0.5		0.2		tr		0.3
Other†	0.3		0.4		0.5		1.0		1.6		3.0		1.1
	100		100		100		100		100		100		100

* Most frequent value K-feldspar plus microcline; P_3 = 39.8%.
† Limonite, chlorite, actinolite, epidote.

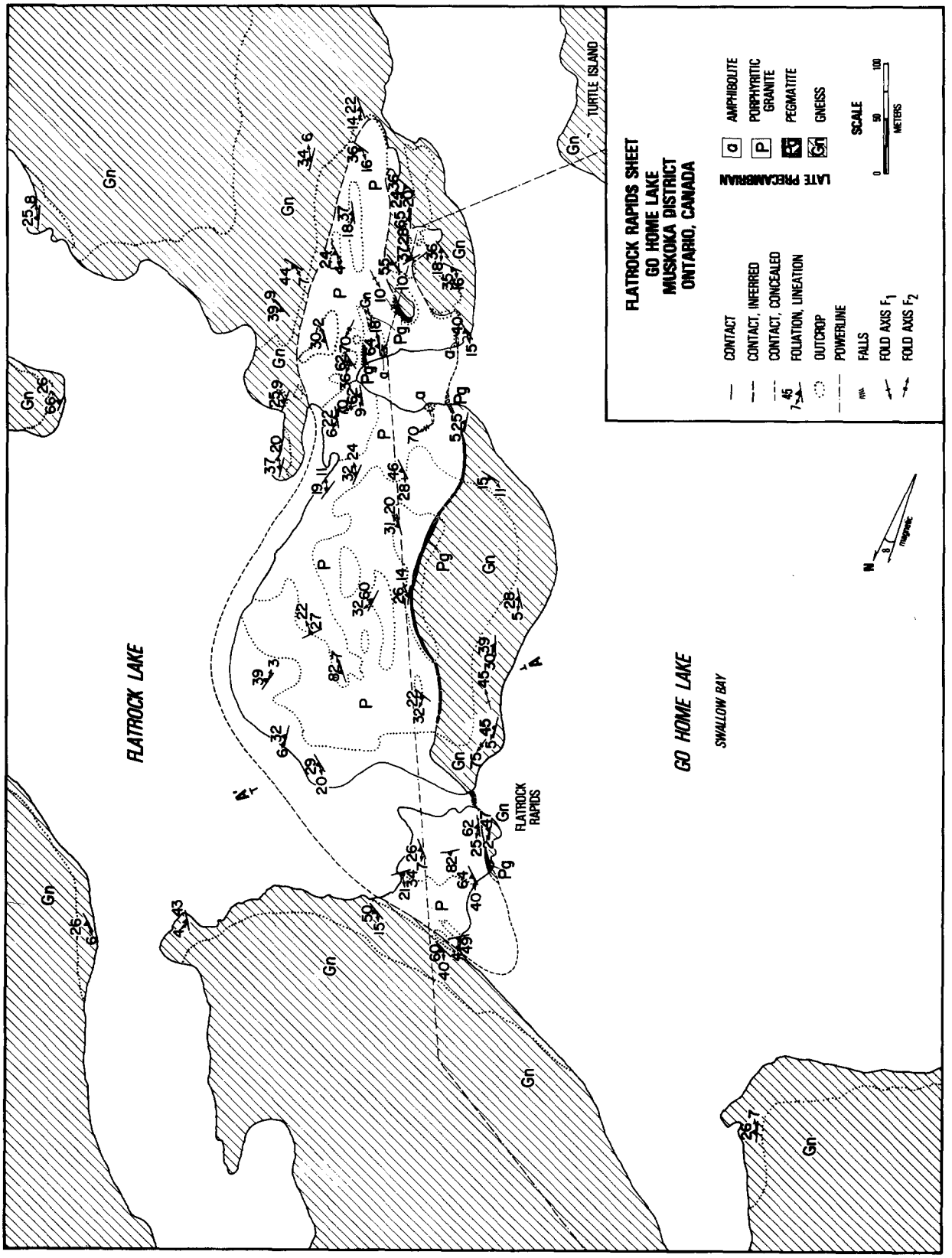

Fig. 2. Geologic map of the Flatrock Rapids area, Muskoka District, Ontario.

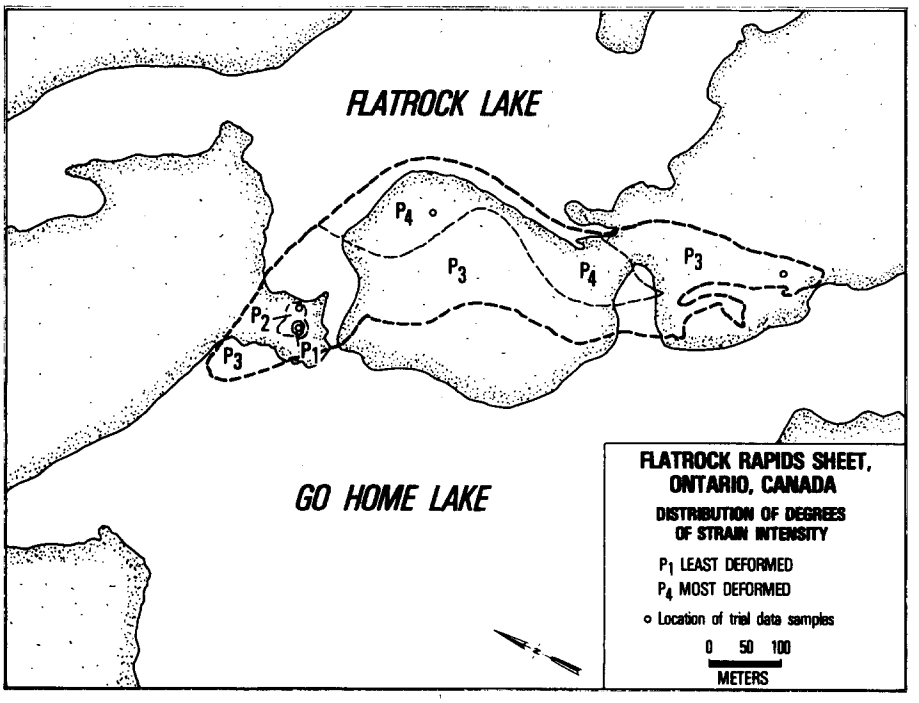

Fig. 3. Aerial distribution of the four ideal degrees of strain intensity in the Flatrock Rapids Sheet.

Table 3. Nature and abundance of megacrysts and groundmass, Flatrock Rapids

Degree of strain intensity	P_1 (1 sample)	P_2 (2 samples)	P_2–P_3 (4 samples)	P_3 (9 samples)	P_3–P_4 (5 samples)	P_4 (2 samples)
Quartz	1–3 mm; anhedral, undulose extinction lamellae (10%)	1–5 mm; anhedral, undulose extinction lamellae (15%)	3–10 mm; anhedral, elongate aggregates, undulose extinction lamellae (10%)	1–10 mm; usually	5–15 mm, anhedral	5–8 mm; elongate
Orthoclase	8–10 mm; subhedral–euhedral, minor quartz veins (45%)	7–50 mm; euhedral to subhedral, graphic intergrowth, Carlsbad twins (40%)	6–30 mm; euhedral to anhedral (15%)	1–5 mm; elongate, anhedral aggregates, undulose extinction lamellae, bubble trails, clear blue–grey, sutured grain boundaries, minor secondary recrystallization, inclusions, locally banded (10%)	aggregates in bands, undulose extinction lamellae, bubble trails, clear blue–grey, secondary recrystallization, inclusions (10%)	anhedral aggregates, clear blue–grey, undulose extinction lamellae (10%)
Microcline			1–5 mm; subhedral twinned (10%)	5–15 mm; polygonized aggregates up to 10	1–5 mm; anhedral aggregates (5%)	absent
				5–15 mm; anhedral aggregates to bands, twinned (30%)	3–15 mm; anhedral aggregates and bands	5–100 mm; anhedral aggrebounded, twinned (30%)
Shape of megacrysts	Euhedral	Euhedral to subhedral		Subhedral to anhedral (elliptical to lensoid)		
% Megacrysts	55	55	35	35	10–30%	10–30%
Groundmass						
% Recrystallization of groundmass	0	10	20	>60%	>80%	>80%
Size of groundmass (mm)	0.25–1.5	0.25–1	2–3	1–2	0.5–2	0.25–2
Degree and nature of groundmass anisotropy	Isotropic to weakly foliated	Foliated, poorly developed lineation		Well foliated and lineated		Well foliated and lineated, banded

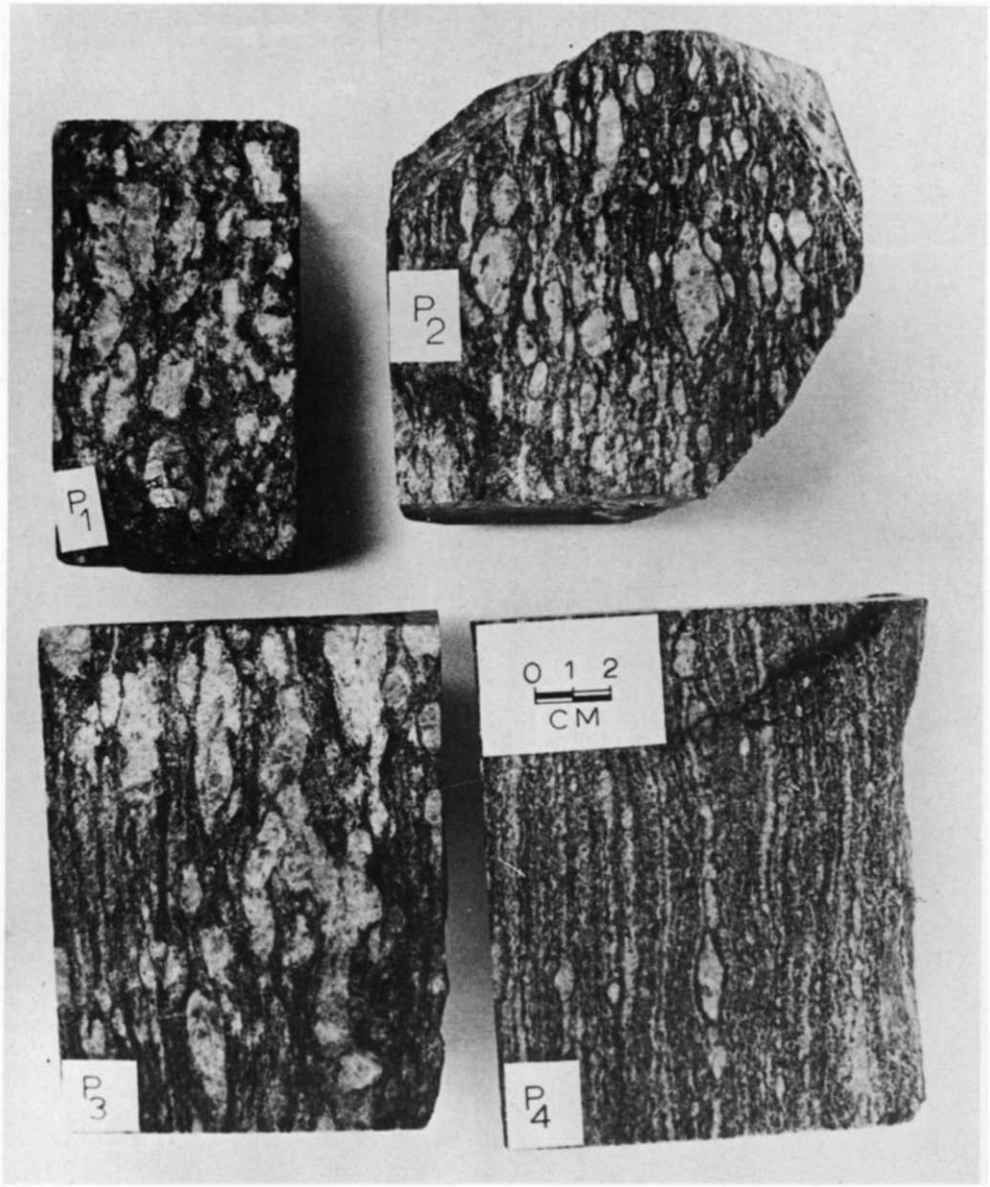

Fig. 4. Idealized degrees of strain intensity in samples of the poryphyritic granite, Flatrock Rapids sheet (P_1 = least deformed).

depending upon the degree of deformation the rock has undergone (see Table 3). Quartz, K-feldspar, plagioclase, biotite, hornblende and a variety of minor accessories constitute the ground-mass minerals which also vary in grain size and degree of crystallization (Table 3).

Four degrees of strain intensity were recognized within the sheet in the field (Fig. 3) The degrees of strain intensity were determined by the overall shape of the phenocrysts and the amount of fabric anisotropy developed within the body. These degrees are designated P_1 (undeformed) through to P_4 (most deformed) and the textural and structural characteristics of each degree is shown in Fig. 4 and described in Table 3. Intermediate stages of strain intensity were also recognized and are so designated.

As the FRS exhibits a metamorphic fabric over most of the area studied, evidence for its intrusive nature rests largely upon: (1) its spatial distribution, (2) the amount, distribution, and type of K-feldspar phenocrysts, (3) the presence and distribution of quartz 'eye' aggregates and (4) the absence of internal features such as comminution structure, cataclasis and mortar structure in the relatively undeformed portions of the body. However, the general degree of fabric development, the concordant to subcordant relations with the wallrock and the absence of chilled contacts suggests that intrusion and thermal metamorphism were probably closely associated in time.

The range of orthoclase plus microcline (total) from 39 to 40% indicates a uniform composition in the FRS relative to that observed in the host gneiss (see Tables 1 and 2). As this mineral group appears uniformly distributed megascopically, even within a given degree of strain intensity in the sheet, it is believed that K-feldspar was converted to microcline within the more deformed parts of the sheet during the deformational process. That the degree of recrystallization in the groundmass is also increased in the more deformed areas supports such an interpretation.

Quartz occurs as 1–15-mm aggregates which make up 20–40% of the FRS, but most often comprises 25–30%. These 'eyes' are ubiquitous in the FRS when compared to the more variable range of distribution for quartz observed in the gneiss (1–50%).

Amphibolite occurs as layers, lenses and pods within the gneiss and to a lesser extent as lenses and pods in the granite. This rock type is particularly abundant along the southern contact between the two units. The amphibolite is a fine-grained, holocrystalline, xenomorphic, granoblastic, foliated unit. Modal values of the rock are given in Table 1. Although not apparent from the mineralogic character of the amphibolite, it is reasonable to assume that the enclaves of this rock type may represent various mafic volcanic units intruded or incorporated within the host units which underwent deformation with the respective host rocks.

One major sheet of pegmatitic granite occurs along the western boundary of the FRS, and a number of smaller dykes of similar composition are associated with this body. The pegmatite is rarely more than 2 m wide and contains quartz and K-feldspar together with occasional muscovite, biotite and tourmaline. Grain size averages 5–10 cm. Other such bodies are concordant to discordant and locally folded with the host rock, and are interpreted as being late-stage intrusives.

STRUCTURE

Penetrative and nonpenetrative macroscopic structures are well developed in the Flatrock Rapids area.

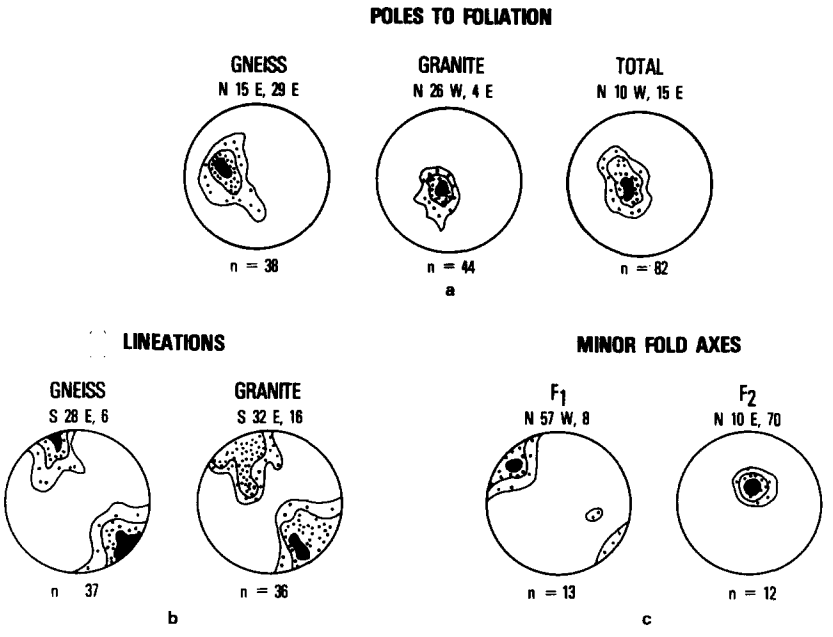

Fig. 5. Structural data from the Flatrock Rapids study area. (a) poles to foliation, (b) mineral lineations, (c) fold axes. All lower-hemisphere, equal-area projections; contours at 5, 10 and 15% points per 1% of area.

Table 4. Descriptive parameters of folds, Flatrock Rapids area, Muskoka District, Ontario (nomenclature after Fleuty 1964, Ramsay 1967)

Criteria	Phase of folding F_1 Major	F_1 Minor (Parasitic)	F_2
Strike and dip of axial surfaces	330–335 (150–155); 10–30	300–310; 10–40	10–35 (190–215); 20–70
Dip of hinge surface	unknown, probably recumbent to gently inclined	recumbent to gently inclined	steeply inclined
Plunge of hinge	gentle	gentle	steep
Interlimb angle	tight to isoclinal	tight to isoclinal	gentle to open
Vergence	northwest	northwest	northward
Class of fold (Ramsay, 1967)	unknown, but probably 2 or 1C, 3	2, with some flattening	1A, 3
Wave length	unknown, but >3 km.	30 cm–1 m	2–5 m
Amplitude	unknown	1–2 m	1 m

Penetrative structures include foliation and lineation as well as two phases of folding. Nonpenetrative structures consist of fault zones and joints.

Secondary mineral foliation and lineation were recognized and recorded in the gneiss unit, the FRS and the amphibolite unit. Foliations include platy mineral alignment and gneissic banding; boudinage, elongate mineral alignment, slickensides, minor fold axes and grain boundary intersections with foliation planes constitute the linear features. As noted in Fig. 5, foliations strike 150–175° and dip 20–30° NE. Similarly, mineral lineations trend either NW or SE with a shallow plunge (10–20°) along or close to the strike of foliation.

Two distinct generations of folds have been recognized in the study area. Table 4 summarizes the nature and characteristics of these fold types (see also Fig. 5). Early, NW-trending folds (F_1) are tight to isoclinal, recumbent to gently inclined and nearly similar in form (Figs. 6a & b). Only parasitic, minor folds of this generation could be observed; the scale of the major folds did not permit direct examination of their form in the area. However, the foliation pattern exhibited by the FRS and gneiss units suggests these units may be folded together in a major, recumbent to gently inclined structure, dipping eastward with a steeply plunging closure on the north end.

Second generation folds (F_2) cross-fold the earlier set along a 010–035° axial-plane trend. The F_2 folds are more steeply plunging than the first generation and consist of flattened buckle folds (Fig. 6c) which verge NW. Type 2 interference patterns (Ramsay 1967) produced by the F_2 cross folding were observed locally (Fig. 2) as well as regionally. The orientation, nature and vergence of the F_1 and F_2 folds in the study area, together with the fabric data, suggest that the overall structure of the FRS is that of a multiply deformed type 2 fold.

Although no large fault zones were directly observed, a major 070° trending linear feature which structurally controls the Go Home River passes a few hundred meters to both the north and south of the area. Harrison (1976) interpreted this feature as a normal fault with the southeast side upthrown. Major lineaments in the area, such as the Go Home River structure, have not been studied in detail (Schwerdtner & Waddington 1978).

Several minor cataclastic zones up to 15 m in length and 1 m in width were observed in the study area. Usually, such zones are subparallel to foliation or cross-cut foliation at low angles and often occur adjacent to pegmatite bodies in the gneiss and granite units. In one case, slickensides (plunge 80°/280°) were observed. Joint analysis was not carried out in this study.

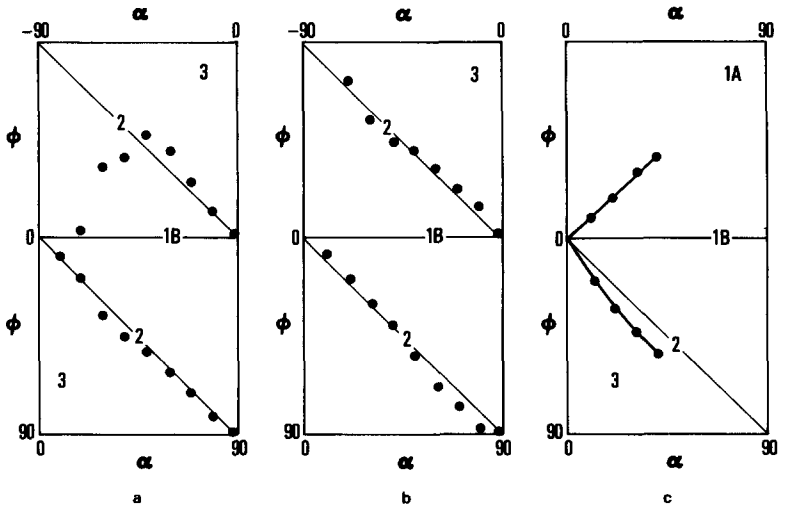

Fig. 6. Classification of folds in study area using method of Hudleston, 1973. (a) and (b) F_1 folds with ϕ scale reversed in upper half, (c) F_2 fold. Diagram depicts ϕ, the dip isogon and α, the angle of dip; see Hudleston (1973) for details.

STRAIN ANALYSIS

Sample preparation

Samples of the deformed granite sheet were prepared for strain analysis in a manner similar to that described by Tobisch *et al.* (1977). This involved sectioning samples along three orthogonal planes, parallel to foliation [designated XY], lineation [YZ], and perpendicular to the other two [XZ], using a diamond saw. As in the study by Tobisch *et al.* (1977), large samples (up to 15 kg) were required where the individual grains and aggregates reached 6 cm or more; also difficulty was encountered in consistent precise cutting of large samples along the planes containing foliation or lineation as the identification of these planes was often difficult on the uncut specimen surface. A trial-and-error method proved successful, however, for determining such surfaces. The completed samples averaged 15 cm per side. After sawing, samples were sprayed with clear plastic for purposes of providing visual contrast between the deformed phenocrysts (strain markers) and the matrix.

Crystal shapes of the deformed grains or aggregates were then traced on to mylar drafting film for each of the three sets of planes. The shape (maximum length and width) and angular relations of the grains to the principal directions of a right-handed Cartesian coordinate system were determined. Definition of grain boundaries proved difficult only in the most deformed samples where 'ellipses' were composed of a mosaic of smaller grains. Grains were not counted in cases where there was any doubt about the definition of the grain boundary; thus, strain values for the more deformed samples no doubt represent minimal values. The time required to cut, spray and count an individual sample is between 10 and 20 h.

A minimum of 50 grains was counted per plane in each sample with 100 grains being counted in the majority of cases. Holst (1977) indicates that 100 markers per plane renders accurate and reproducible results in this type of analysis. Planes with an insufficient number of markers were serially sectioned to provide an adequate quantity for study.

Comparison of analytical methods

Samples representing four degrees of strain intensity (P_1–P_4, with increasing deformity) within the FRS were initially analysed using three different analytical techniques in order to determine which methods were most accurate, reproducible and expedient (see Fig. 3 for sample locations). The techniques used in this analysis were: (1) the ratio of principal axes/angle R_f/ϕ (Ramsay 1967, p. 209) and the R_s value (Dunnet 1969); (2) the centre point (Ramsay 1967, p. 195) and (3) the shape factor grid or polar plot (Elliott 1970). Data was displayed by: (1) the deformation plot (k value, Flinn 1965, Ramsay 1967); (2) the three axis, planar diagram (Hossack 1968, Nadai 1968, Owens 1974, Hsu 1966) and (3) the R_f/ϕ and d/α plots (Ramsay 1967).

A FORTRAN IV computer program was written to permit calculation of the mean values of strain ellipsoid principal axes and planes and their ratios (X/Y, Y/Z, X/Z). This program also calculated values for and displayed (cathode ray terminal) the R_f/ϕ plot, the polar plot used in the shape-factor grid analysis and the three axis planar diagram. In addition, the ratios of the principal axes and their angular relations were analysed on a program provided by A. W. B. Siddans (Dunnet & Siddans 1971) which calculated a best-fit strain ellipsoid, Flinn k values, and overall percentages of shortening and elongation. This program also calculated the 'level of internal inconsistency' for a given data set and this parameter was used to compare the accuracy of results for the various methods.

As with all analytical strain techniques, certain assumptions are inherent to the methods and such is the present case. All of the methods noted above assume finite homogeneous strain for the body (Schwerdtner 1976). Also, it is recognized that the feldspar strain markers were originally non-spherical (rectangular) with an initial shape that can be approximated within an ellipse. A random initial fabric has also been assumed and it was for that reason that the R_f/ϕ and shape factor methods were selected. The centre point method was used to test whether the strain markers deformed homogeneously with their matrix. These techniques cannot determine either the rotational component of deformation or the volume change during deformation.

Results from the XZ plane of samples exhibiting the four 'ideal' degrees of strain intensity (P_1 to P_4) using a Ramsay (1967) R_f/ϕ diagram are shown in Fig. 7. This method is reasonably accurate for XZ faces as may be noted by the level of internal inconsistency (Table 5) and may be used fairly efficiently. However, considerable subjectivity may be involved in depicting the shape of the enclosing envelope for XY and YZ faces.

Values of R_s were also calculated using the method of Dunnet (1969) and results for four samples are shown in Fig. 8. This method provided the most reliable and sensitive results (Table 5) and was used in the overall analysis of the FRS.

Data for the centre point technique (Ramsay 1967, p. 195) are presented in Fig. 9. The subjectivity involved in the determination of centre points with increasing degrees of strain intensity accounts for the impreciseness of the method (Table 5) and it was abandoned.

Figure 10 shows the results for the XZ faces from the four samples using the polar plot of Elliott (1970). One problem presented by this method was that of determining a point which could be used in unstraining the data. Typically the orientation of an initial fabric point (I.F.P., after Holst 1982) may be recognized for a strained body by an indentation in the base of the contour envelope which develops with straining (Elliott 1970, fig. 15). As recognition of obvious primary fabric such as bedding was not possible in the rocks studied here (Fig. 9), it became necessary to seek alternative methods for unstraining the samples. One method suggested was to assume that the centre of the contour envelope rep-

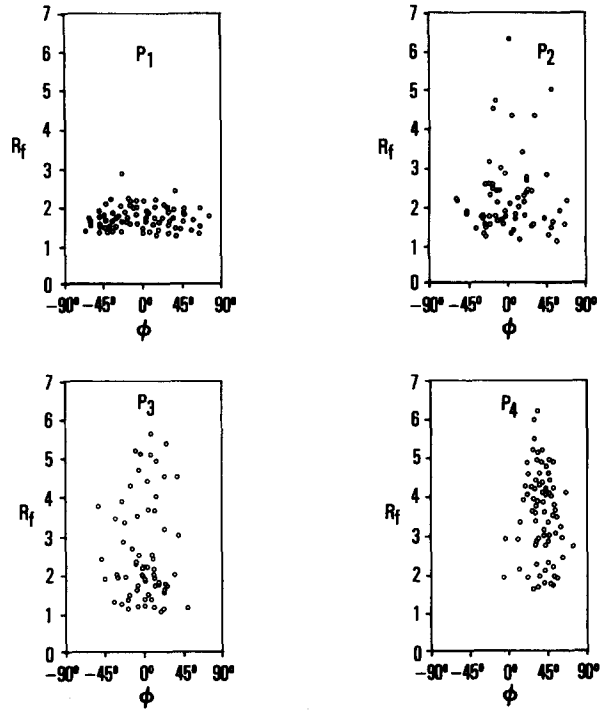

Fig. 7. Comparative strain data for ideal degrees of strain intensity using the particle axis/angle (R_f/ϕ) method of Ramsay 1967. Values are in axial ratios (R_f) for XZ faces vs ϕ, the angle between the long axis of the particle and a reference direction.

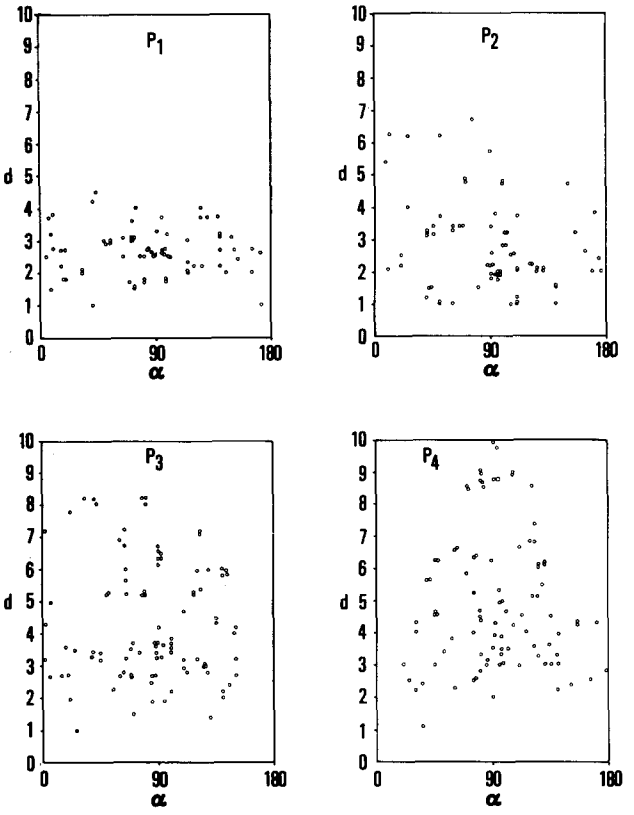

Fig. 9. Comparative strain data for ideal degrees of strain intensity using the centre point method (Ramsay 1967). Values of d are unspecified units of distance between adjacent particle centres for XZ faces and α the angle between lines connecting centres and a reference direction.

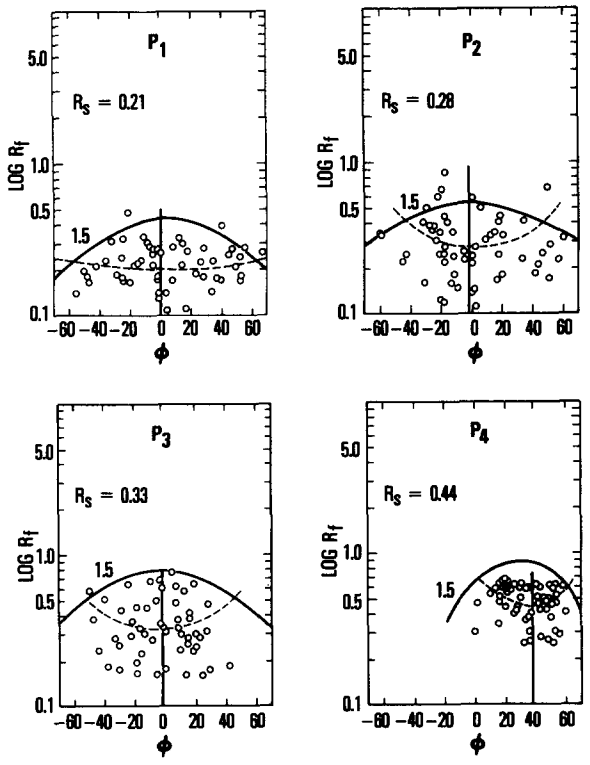

Fig. 8. Comparative strain data for ideal degrees of strain intensity using the R_s method (Dunnet 1969, Dunnet & Siddans 1971). Values are log R_f (axial ratio) and ϕ, the angle between the long axis of the particle and a reference direction. Dashed line represents 50% of data curve.

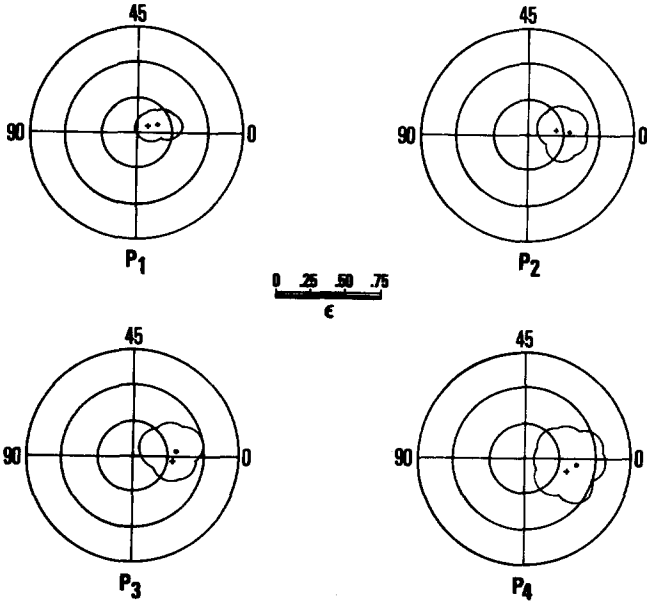

Fig. 10. Comparative strain data for ideal degrees of strain intensity using polar plot of Elliott (1970). Values plotted are $\epsilon = 1/2 \ln (R_f)$ and $\phi = 20$ from 0 to 90° for XZ faces. Pluses represent statistical centre of values in contour bag; dots represent geometric centre. Contour level is 2% of data.

Table 5. Results of comparative strain analyses on deformed feldspar aggregates from four samples representing ideal degrees of strain intensity, Flatrock Rapids Sheet, Ontario. (See text for explanation of methods)

Degree of strain intensity	P_1	P_2	P_3	P_4	Level of internal inconsistency (all faces)
Method					
R_f/ϕ					
R_{fn} max	2.99	4.98	5.38	6.02	29
R_f min	1.03	1.01	1.05	1.56	9.5
R_s	0.21	0.28	0.33	0.44	
Centre point max/min	4.3	6.7	8.2	11.02	48%
Polar plot Centre	1.33	1.6	1.6	1.7	5%
Sample (all faces)					
k-Flinn	1.0	0.92	0.84	0.68	
Three axis planar					
ν	0.04	0.4	0.6	0.8	
ϵ_s	0.61	0.77	1.6	1.9	
Computed best-fit ellipsoid	1.24:1.0:0.91	1.53:1.0:0.61	1.7:1.0:0.5	1.7:1.0:0.39	
Per cent flattening	21	25	31	38	
Per cent elongation	22	23	21	24	

resented a reasonable estimate of the I.F.P. (P. Hudleston, pers. comm.). Unstraining is then accomplished by simply moving this point back to the origin of the polar plot. It became apparent, however, that this point would only crudely account for the distribution of points within the diagram and, therefore, the average value of strain (ϵ) was used as the I.F.P. with unstraining accomplished by moving that point to the origin of the polar plot.

Holst (1977, 1982) has examined and quantified this procedure and shown it to produce accurate and reproducible results although consistently overestimating strain because of the 'geometrical consequence of the nature of the equation which define the deformation path of an ellipse plotted on the Elliott diagram' (Holst 1977, p. 104). Corrections for this overestimation are easily made (Holst 1977). Use of the average value of ϵ in the Elliott (1970) method gives very consistent results (Table 5) and was also used in the overall analysis of the FRS. The value of P_1 in Fig. 9 shows strain in the least deformed sample.

Strain distribution, FRS

Strain determinations were carried out on feldspar grains in 28 samples of the FRS and 10 samples of the gneiss from the Flatrock Rapids area using the R_f/ϕ, R_s and polar plot methods. The results were displayed on deformation plots and three axis planar diagrams as discussed above.

Figure 11 represents the results of analyses on 28 samples of feldspar from the FRS together with ten samples from the gneiss on a Flinn deformation plot. Flattening strain appears dominant in areas exhibiting the higher degrees of strain intensity in the FRS (compare Figs. 3 and 11) while constrictive strain appears most common in the gneiss.

Contoured k-values for the FRS are depicted in Fig. 12, contoured values of strain magnitude are shown in Fig. 13 and contoured values of R_s are shown in Fig. 14. These diagrams illustrate that areas with the greatest calculated strain magnitude (highest ϵ_s) correspond well with the greatest degrees of strain intensity observed and analysed in the FRS (Fig. 3). The dominant type of deformation is flattening which is best developed in an arcuate band adjacent to, but not coincident with, the northern boundary of the FRS and a small, circular area in the south central portion of the sheet. Areas with higher degrees of strain intensity correspond well with areas of high strain magnitude (Figs. 11 & 12). Data

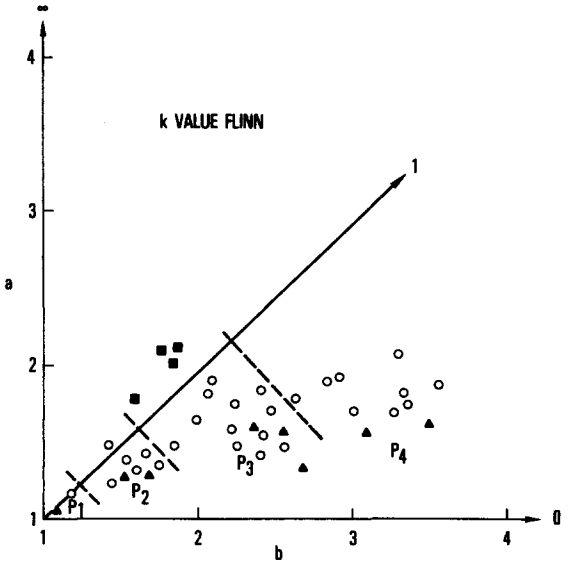

Fig. 11. Palaeostrain data from the study area using the deformation plot of Flinn. $a = \lambda_1^{1/2}/\lambda_2^{1/2}$ and $b = \lambda_2^{1/2}/\lambda_3^{1/2}$. P_1–P_4 refer to ideal degrees of strain intensity. Squares represent gneiss samples, circles represent FRS feldspar samples, and triangles represent matrix mica samples in the FRS.

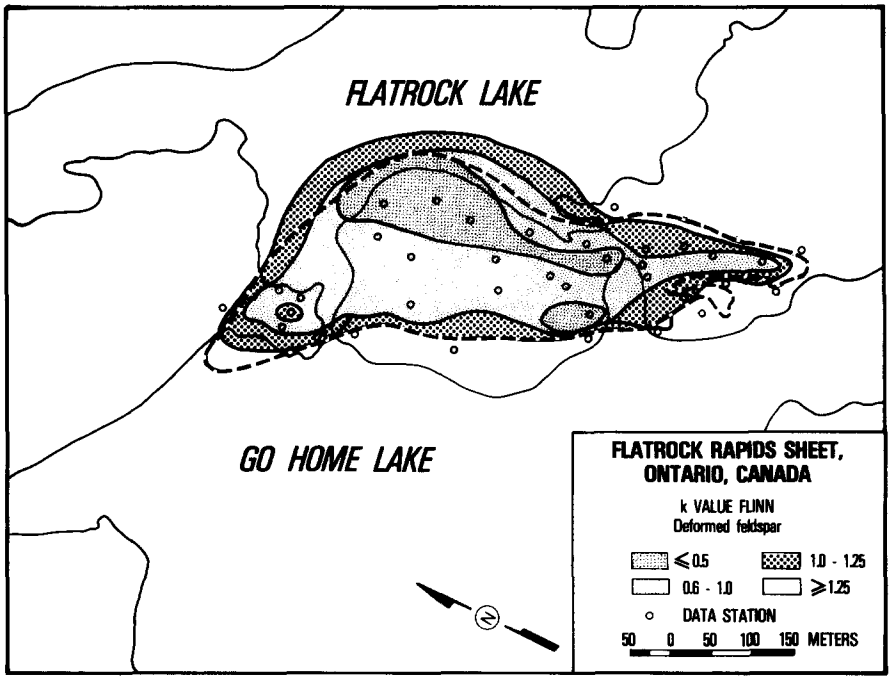

Fig. 12. Map of study area showing contoured values of $k = (a - 1)/(b - 1)$ (after Flinn 1965).

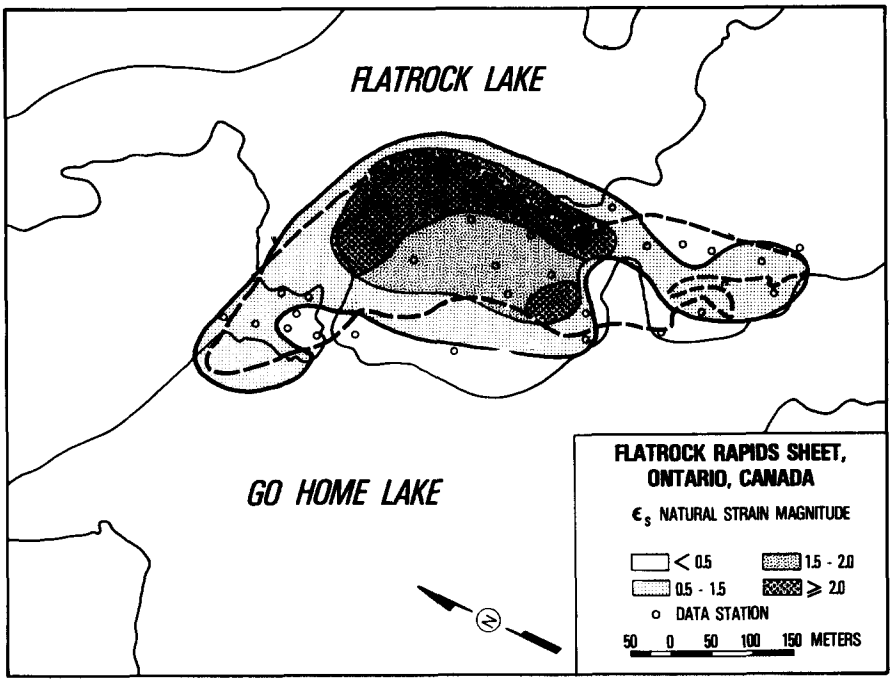

Fig. 13. Map of study area showing contoured values of ϵ_s, strain magnitude, which is a measure of the intensity of the distortional component of strain; see Nadai (1968) for details, as well as text.

from Fig. 11 indicate that the more intense strain fabric developed from a less well-developed strain fabric with a k value near unity (Table 5). The initial fabric in the gneiss can only be inferred to have been more constrictional than the present fabric given the syndeformational history interpreted for the gneiss and the FRS.

High strain gradients were observed along the arcuate northern border and south central portions of the FRS (Fig. 13). The distribution of these gradients appears related to the folding history of the FRS and is discussed below.

Strain in the FRS matrix

Strain determinations were carried out on biotite clots from eight samples of the FRS to determine whether the matrix material had deformed homogeneously with the feldspar grains. The results of this analysis are shown in Fig. 11 and Table 6. Greater strain values (flattening) were consistently measured from the biotite clots than the feldspar grains except in the 'least deformed' state (P_1). The tablet shape of the feldspar grains may account for the 'initial' values measured in these minerals grains.

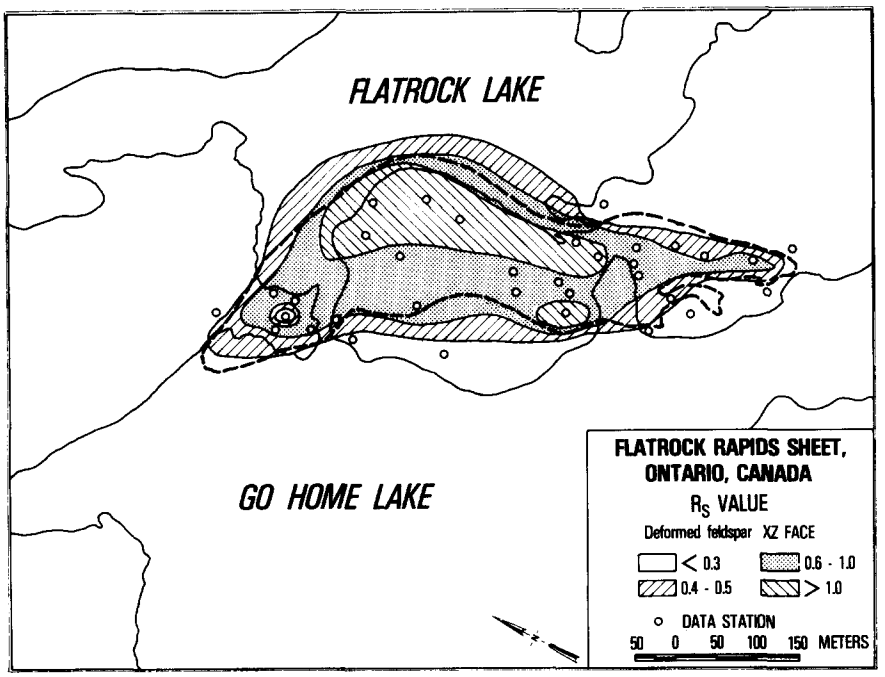

Fig. 14. Map of study area showing contoured values of R_s after the method of Dunnet (1969) and Dunnet & Siddans (1971).

However, the persistently higher strain values for biotite clots with increased degrees of strain intensity indicate either (1) the methods of measurement are inconsistent or (2) that the feldspar did not deform homogeneously with the FRS matrix because of either nonrandom initial fabric or competency contrasts between the platy feldspar grains and matrix during deformation.

Inconsistent measurement is a distinct possibility to account for the data observed, particularly as discrete limits to the biotite clots were often difficult to distinguish. Also, De Paor (1979) has discussed various limitations of the R_f/ϕ technique of strain analysis which include factors such as nonrandom initial fabric distribution as well as ductility contrasts between deformed objects and the matrix. Although both of these conditions might hold in the present study, the fact that results from several methods show consistently greater values for biotite than feldspar, indicates that methodology alone probably does not account for the strain variances observed.

Ramsay (1967, pp. 216–221) discussed the problems of measuring strain in rocks with nonrandom initial fabrics. However, examination of the value of sample P_1 in Fig. 9 suggests that the initial fabric in the FRS was close to random (Elliott 1970, pp. 2223–2224). Ramsay (1967, pp 221–226) also discussed the behaviour of competent objects in a ductile matrix and particularly drew attention to the application of studies by Jeffrey (1922) and Taylor (1973) involving grain rotations which might be applicable to igneous fabrics. As rotation of feldspar phenocrysts within the matrix was not observed, nor could the rotational component of deformation be measured, a competency difference between the matrix and the grains is suggested. This difference is further supported by the high level of inconsistency in the centre point method analysis.

Table 6. Comparative strain analysis, matrix biotite clots and feldspar aggregates, Flatrock Rapids Sheet, Ontario

Sample	Degree of strain intensity	Mineral	R_f/ϕ (XZ max)	R_s (XZ)	ν	ϵ_s
4	P_1	Feldspar	3.0	0.28	0.04	0.4
		Biotite	0.3		0.3	0.3
10	P_2	Feldspar	4.9	0.45	0.4	0.5
		Biotite	6.1		0.5	0.6
35	P_2	Feldspar	4.7	0.37	0.3	0.6
		Biotite	6.0		0.4	0.8
9	P_3	Feldspar	5.2	0.60	0.4	1.8
		Biotite	7.9		0.6	2.2
21	P_3	Feldspar	5.4	0.62	0.6	1.5
		Biotite	8.9		0.8	1.9
45	P_3	Feldspar	6.1	0.82	0.6	1.6
		Biotite	11.3		0.9	2.9
29	P_4	Feldspar	5.7	1.13	0.6	2.6
		Biotite	12.8		0.9	2.7
43	P_4	Feldspar	6.0	1.24	0.8	2.3
		Biotite	12.0		0.9	3.6

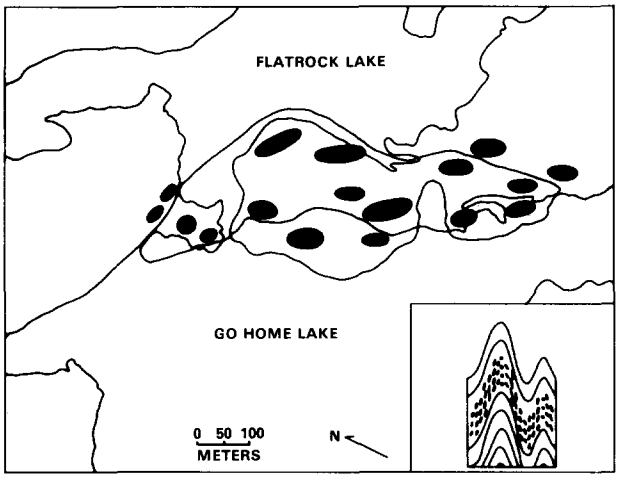

Fig. 15. Map of study area showing idealized construction of two-dimensional strain ellipse patterns for XZ planes, projected onto a horizontal plane. Inset shows ideal distribution of two-dimensional strain ellipses for similar (class 2) fold (Ramsay, 1967).

DISCUSSION

Fabric elements in, as well as contact relations between, rock units in the Go Home Lake study area suggest all the rock units were deformed penecontemporaneous with the intrusion of the FRS into the host gneiss. This deformation resulted in development of regional-scale, recumbent, isoclinal folds with similar (type 2) geometry and NW-trending hinge-surface traces A metamorphic fabric and the general elongate shape of the FRS were probably generated during this deformation.

A second deformational event, also of regional extent, then modified the geometry of the F_1 folds producing a type 2 fold interference pattern. F_2 folds are steeply plunging northward with steeply inclined hinge surfaces. These open, class 1A and 3 folds have NE-trending hinge surface traces and verge northward. It is believed this deformation modified the shape of the FRS to its present crescentic shape and produced the structural fabric and strain elements analysed.

Fabric analysis suggests that the present configuration of the FRS resulted from modification of a nearly recumbent, isoclinal similar fold form by contractional, buckle(?) folding. Strain analysis confirms the basic similar (class 2) fold geometry of the FRS and the patterns of strain intensity and strain magnitude suggest modification of this form by shortening. An idealized construction depicting the strain pattern of the FRS is shown in Fig. 15.

The patterns of strain intensity and strain magnitude observed in the FRS are not expected to be ideal owing to competency (ductility) contrasts during deformation. Such contrasts have been demonstrated between the matrix and strain markers in the FRS and can be reasonably assumed between the FRS and the gneiss because of differences in fabric anisotropy, which may account for the pattern of strain gradients observed.

Consideration of the timing of deformations at Go Home Lake, the relationship of the FRS structure to the regional tectonic framework, and the possible analysis of the rotational deformation component (e.g. Kligfield *et al.* 1981) awaits further study.

Acknowledgements—The author wishes to thank Mr. Chahe Sabbagh who assisted with the field work, Mr. Steven Olson who worked with me on the computer programming, and Mr. Leroy Warren and Mrs. Linda Marston who helped with the drafting. Dr. W. M. Schwerdtner not only brought the problem to the attention of the author, but offered advice throughout the course of the project. Early versions manuscripts were read by Drs. W. M. Schwerdtner, T. Holst and P. Hudleston as well as two anonymous reviewers. The project was supported in part by grants from the National Resources Council of Canada and the Computer Center at the University of Minnesota, Duluth.

REFERENCES

Allison, I. 1975. Strain variations in a deformed granite (Abs). *Geol. Soc. Am. Abs.* with *Programs* **7** (6), 711.

Bennett, P. J. 1975. The deformation of the northern half of the Brandy Lake Complex, Port Carling, Ontario. Unpublished thesis, Department of Geology, University of Toronto, Ontario.

Burg, J. P. & Laurent, P. H. 1978. Strain analysis of a shear zone in a granodiorite. *Tectonophysics* **47**, 15–42.

Coward, M. P. & James, P. R. 1974. The deformation patterns of two Archean greenstone belts in Rhodesia and Botswana. *Pre-Cambrian Res.* **1**, 235–258.

Davidson, D. M. Jr. 1980. Emplacement and deformation of the Archean Saganaga Batholith, Vermilion District, northeastern Minnesota. *Tectonophysics*, **66**, 179–195.

De Paor, D. G. 1979. Some limitations of the R_f/ϕ technique of strain analysis. *Tectonophysics* **64**, T29–T31.

Dunnet, D. 1969. A technique of finite strain analysis using elliptical particles. *Tectonophysics* **7**, 117–136.

Dunnet, D. & Siddans, A. W. B. 1971. Non-random sedimentary fabrics and their modification by strain. *Tectonophysics* **12**, 307–325.

Elliott, D. 1970. Determination of finite strain and initial shape from deformed elliptical objects. *Bull. geol. Soc. Am.* **81**, 2221–2236.

Fleuty, M. J. 1964. The description of folds. *Proc. Geol. Ass.* **75**, 461–492.

Flinn, D. 1965. On the symmetry principle and the deformation ellipsoid. *Geol. Mag.* **102**, 36–45.

Harrison, C. 1976. Structural analysis of the GO HOME BAY area, Muskoka District, Ontario. Unpublished thesis, Department of Geology, University of Toronto, Toronto, Ontario.

Hewitt, D. F. 1967. *Geology and Mineral Deposits of the Parry Sound–Huntsville Area.* Ont. Dept. Mines Geol. Rept. **52**.

Holst, T. B. 1977. The determination of finite grain in rocks: the role of primary fabric. Unpublished thesis, University of Minnesota, Minneapolis, Minnesota.

Holst, T. B. 1982. The role of initial fabric on strain determination from deformed ellipsoidal objects. *Tectonophysics* **82**, 329–350.

Hossack, J. R. 1968. Pebble deformation and thrusting in the Bydgin area (Southern Norway). *Tectonophysics* **5**, 315–339.

Hsu, K. C. 1966. The characteristics of coaxial and non-coaxial strain paths. *J. Strain Analysis* **1**, 216–222.

Hudleston, P. J. 1973. Fold morphology and some geometrical implications of theories and fold development. *Tectonophysics* **16**, 1–46.

Jeffrey, G. B. 1922. On the motion of ellipsoidal particles immersed in a viscous fluid. *Proc. R. Soc.* **102A**, 161–179.

Kligfield, R., Carmignani, L. & Owens, W. H. 1981. Strain analysis of a Northern Apennine shear zone using deformed marble breccias. *J. Struct. Geol.* **3**, 421–436.

Lumbers, J. B. 1974. Geologic Map of the Burwash region (1:126,720). Ontario Div. Mines Map 2271.

Nadai, A. 1968. *Theory of Flow and Fracture of Solids* (2nd edition). Engng Sci. Monograph, McGraw Hill, New York.

Nicolas, A., Bouchez, J. L., Blaise, J. & Poirer, J. P. 1977. Geological aspects of deformation in continental shear zones. *Tectonophysics* **42**, 55–73.

Owens, W. H. 1974. Representation of finite strain state by three-axis planar diagram. *Bull. geol. Soc. Am.* **85**, 307–310.

Potter, C. J. 1976. Deformational and compositional variations in shear zones in the Kinsman Quartz Monzonite. Unpublished thesis, Brown University, Providence, Rhode Island.

Ramsay, J. G. 1967. *Folding and Fracturing of Rocks*. McGraw-Hill, New York.

Ramsay, J. G. & Graham, R. H. 1970. Strain variations in shear belts. *Can. J. Earth Sci.* **7**, 786–813.

Ramsay, J. G. & Wood, D. S. 1973. The geometric effect of volume change during deformation processes. *Tectonophysics* **16**, 273–277.

Ramsay, J. G. & Allison, I., 1979. Structural analysis of shear zones in alpenised hercynian granite. *Schweiz. miner. petrogr. Mitt.* **59**, 251–279.

Schwerdtner, W. M. 1976. A problem of nomenclature in paleostrain analysis. *Tectonophysics* **30**, T1-T2.

Schwerdtner, W. M. 1977. Geometric interpretation of regional strain analysis. *Tectonophysics* **39**, 515–531.

Schwerdtner, W. M., Bennett, P. J. & James, T. W. 1977. Application of *L-S* fabric scheme to structural mapping and paleostrain analysis. *Can. J. Earth Sci.* **14**, 1021–1032.

Schwerdtner, W. M. & Waddington, D. H. 1978. Structure and lithology of the Muskoka–Southern Georgian Bay region, central Ontario. In: *Toronto '78 Field Trip Guidebook* (edited by Currie, A. L. & Mackasey, W. O.) Geol. Ass. of Canada, 204–212.

Schwerdtner, W. M., Stone, D., Osadetz, K., Morgan, J. & Stott, G. M. 1979. Granitoid complexes and the archean tectonic record in the southern part of northwestern Ontario. *Can. J. Earth Sci.* **16**, 1965–1977.

Streckeisen, A. L. 1967. Classification and nomenclature of igneous rocks: final report of an inquiry. *Neues Jb. Geol. Paläont. Abh.* **107**, 144–240.

Taylor, G. I. 1973. The motion of ellipsoidal particles in a viscous fluid. *Proc. R. Soc.* **103A**, 58–61.

Themistocleous, S. G. & Schwerdtner, W. M. 1977. Estimates of distortional strain in mylonites from the Greenville Front tectonic zone, Tomiko area, Ontario. *Can. J. Earth Sci.* **14**, 1708–1720.

Tobisch, O. T., Fiske, R. S., Sacks, S. & Taniguchi, D. 1977. Strain in metamorphosed volcaniclastic rocks and its bearing on the evolution of orogenic belts. *Bull. geol. Soc. Am.* **88**, 23–40.

Wynne-Edwards, H. R. 1972. The Greenville Province. In: *Variations in the Tectonic Styles in Canada* (edited by Price, R. A. S. & Douglas, R. J. W.). Spec. Pap. geol. Ass. of Can. No. 11, 263–334.